Wedge-Shaped Scintillation Crystals for Positron Emission Tomography

D. Schmitt, R. Lecomte, and E. LeBel

Department of Nuclear Medicine and Radiobiology, Centre Hospitalier Universitaire, Université de Sherbrooke, Sherbrooke, Québec, Canada

The use of wedge-shaped scintillation crystals for positron emission tomography is re-evaluated with the aim of delimiting its range of benefit. A linear attenuation simulation model is used to generate the detector geometric aperture functions, and the investigation is carried out in terms of a newly introduced shape-independent definition of the spatial resolution, the "spectral resolution." Contrary to previous expectations, it is concluded that shaped crystals do not improve the performance of high resolution detection systems, either with or without intercrystal septa. However, wedges are found to be useful for lower resolution systems and the boundaries of applicability are estimated for NaI, BaF_2, GSO, and BGO scintillators.

J Nucl Med 27:99–104, 1986

The current trend in positron emission tomography (PET) towards high spatial resolution has led to the use of narrower detectors (*1–3*), causing a significant increase in interdetector spillage and resulting in less uniform spatial resolution over the camera field-of-view. In an attempt to solve this problem, it was recently suggested to reshape scintillation crystals to have a wedge-shaped front end (*4–7*). Claims of significant improvement in both sensitivity and resolution were made by Cho et al. (*4*), who carried out Monte Carlo simulations where events were classified according to the detector of interaction in order to compare the flat and wedge-shaped crystals. This approach gives little insight on the actual resolution improvement, and moreover, appears fallacious since only the front face of one detector is subjected to irradiation even for obliquely incident gamma rays, resulting in large functions of the detector volume being ignored. The geometric aperture function of coincident detector pairs is a more appropriate description for a study of geometrically different setups (*6–8*). The aperture function is directly dependent upon the detector geometry and intrinsic parameters of the camera such as the spatial resolution, and the detection efficiency are readily available from it. The aim of the present paper is to extend the investigation of shaped crystal in order to define their range of benefit.

Received Feb. 21, 1985; revision accepted Sept. 18, 1985.

For reprints contact: Roger Lecomte, PhD, Dept. of Nuclear Medicine, Centre Hospitalier Universitaire, University of Sherbrooke, Sherbrooke, Québec, Canada J1H 5N4.

DETECTOR CONFIGURATION AND SIMULATION MODEL

An illustration of the detector array model used in the calculations is shown in Fig. 1. The investigation was mostly carried out for bismuth germanate (BGO) scintillators and tungsten (W) septa, but results were also obtained for sodium iodide (NaI), barium fluoride (BaF_2), and gadolinium orthosilicate (GSO) scintillators.

In this work, a simulation model previously introduced by Lecomte et al. (*8*) and independently applied by Holmes and Ficke (*6*) and by Lupton et al. (*7*) was used to generate the geometric aperture functions. The model is based on the calculation of the first interaction probability as expressed by the narrow beam attenuation of gamma rays caused by both photoelectric absorption and Compton scattering. The differential detection efficiency curve (or "intrinsic aperture function") of a given detector embedded in an array is calculated as the probability of incident 511 keV gamma rays having their first interaction in this detector. The coincidence aperture function is then computed by convolving the differential efficiency curves of opposing detectors. As Fig. 2 shows, aperture functions cal-

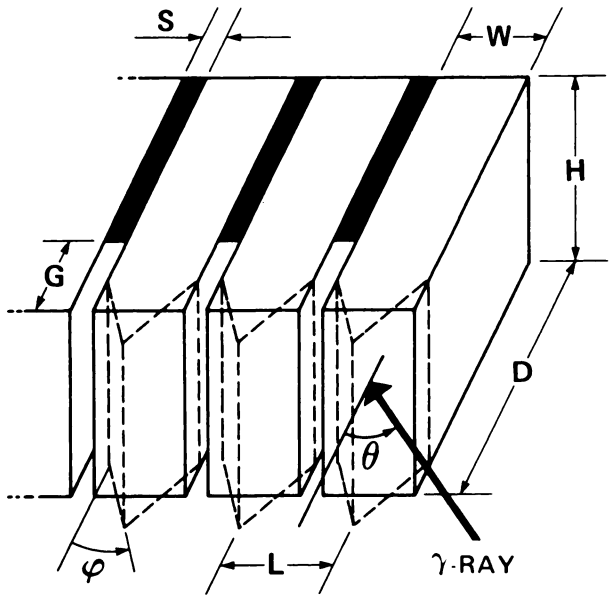

FIGURE 1
Model of detector array

culated from the linear attenuation model are in good agreement with those calculated from Monte Carlo simulations with an energy threshold set above the Compton edge. Since only the annihilation photon first interactions are considered in the linear attenuation calculations, the purely geometric component of the aperture function is obtained. It was decided not to include in the analysis the effect of the other sources of blurring contributing to the experimentally measured aperture functions: on one hand, Compton scattering in the detector array, which is dependent on the detector geometry, is shown to have little effect on the shape of the aperture function; on the other hand, sources of blurring caused by the source (annihilation photon non-colinearity, positron range in the source, size of the source, etc . . .) are independent of the detector geometry and do not alter the geometric contribution to the aperture function. Thus, we assume that the trends in efficiency and resolution of the detection system are adequately handled by the geometric aperture function and that there is no advantage to smear it out with some smoothing function to perform a comparative study of the detector geometry. For comparison purposes with experimental aperture functions, the geometric aperture functions can always be convolved with a smoothing function accounting for the other sources of blurring.

RESOLUTION ESTIMATE

It is common to quote the spatial resolution as the full width at half maximum (FWHM) of the aperture function. Although the FWHM value is very convenient to use, it is not a satisfactory estimate of the resolution of aperture functions since it does not take into consideration the shape of the distribution. For this reason, the full width at tenth of maximum (FWTM) of the aperture function is frequently quoted together with the FWHM (*7,9,10*). In our view, the spatial resolution can be better assessed by the "spectral resolution" R which was previously introduced as (*8*):

$$R = \frac{1}{\int_\nu [MTF(\nu)]^2 d\nu} = \frac{\left[\int_x f(x)dx\right]^2}{\int_x [f(x)]^2 dx} \qquad (1)$$

where f(x) represents the coincidence aperture function and MTF(ν) is its modulation transfer function. This quantity is an interesting and important measure worthy of elaboration. Its significance is better appraised if the detection system is thought of as a spatial filter having a spectral response and a power spectrum given by MTF(ν) and $[MTF(\nu)]^2$, respectively. Then,

$$N_e = \int_\nu [MTF(\nu)]^2 d\nu \qquad (2)$$

is interpreted as the aperture function equivalent power bandwidth, or "equivalent passband," a concept used

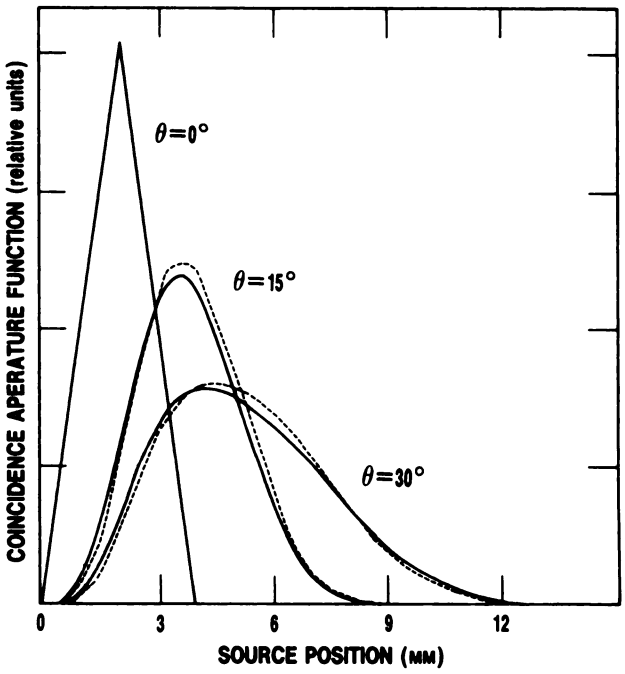

FIGURE 2
Coincidence aperture functions obtained from linear attenuation model and from Monte Carlo simulation for an array of close-packed flat BGO detectors. An energy threshold of 500 keV was used in Monte Carlo simulation. (—) Linear attenuation; (- - -) Monte Carlo (500 keV); D = 25 mm; W = L = 4 mm; Flat face. (See Fig. 1 for description of parameters)

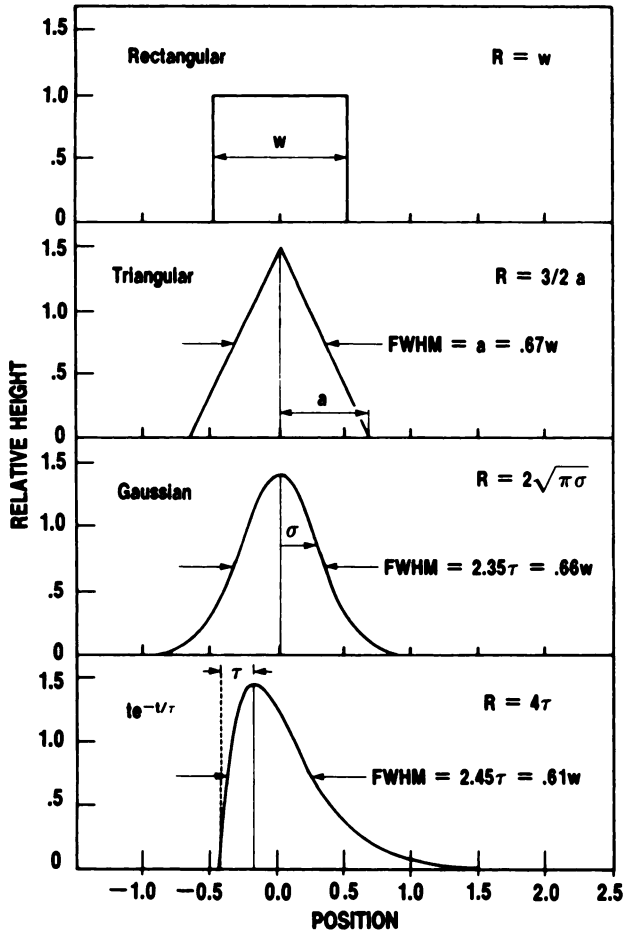

FIGURE 3
Examples of aperture functions with equal spectral resolution R. Functions have been scaled to unit area and centered on median of distribution

extensively to describe sharpness in optical and radiological images (*11*,*12*). From the reciprocity theorem, it follows that R can be interpreted as a spatial domain descriptor defining the width of an equivalent rectangular shaped aperture function with uniform transmission. Therefore, the transmission characteristics of largely different aperture functions with complicated blurring behaviour can be reduced to their equivalent width through Eq. (1) and then be directly compared; the same does not hold for FWHM and FWTM estimates, unless the aperture functions have rigorously identical shapes. Figure 3 shows examples of aperture functions with different shapes and FWHM values, but having equal spectral resolutions R and equivalent power transmission characteristics. Calculated aperture functions for flat and wedge-shaped BGO scintillators are also presented in Fig. 4 together with their measured spectral resolution. Note that the extension of the spectral resolution definition to the two-dimensional point spread function of reconstructed aperture functions is straightforward.

RESULTS AND DISCUSSION

Without Septa

In this section, it was assumed that points were not added onto the detector flat faces, but that the crystals were reshaped with wedges as shown in Fig. 1 in order to compare geometries with equal detection efficiencies. In Figs. 5 and 6, the spectral resolution of the calculated aperture functions is plotted as a function of incidence angle for 4-mm and 8-mm-wide close-packed detectors, respectively. These curves clearly show that the detector depth is the geometrical parameter that has, by far, the most significant effect on the resolution uniformity across the field-of-view of the tomograph. The improvement in uniformity gained by reducing the depth is obtained at the expense of a considerable drop in efficiency, however, the overall array efficiency in coincidence decreases from 95% to 73% and to 38% for the 40-mm, 20-mm and 10-mm detector depths, respectively.

Shaping the crystals does not significantly alter the resolution uniformity. Nevertheless, improvements of up to 0.5 mm (or ~10%) in resolution are reached when using 30° wedges with 8-mm-wide crystals. No such improvement is observed for the 4-mm-wide detectors. This is in evident disagreement with the expectations of resolution and uniformity improvement claimed by Cho et al. (*4*) for narrow-width detectors. There appears to be a decreasing incentive in using pointed crystals in a close-packed geometry as the interdetector distance is reduced (see Fig. 7). This is easily understood if one considers the trivial detector volumes involved in reshaping the front face of crystals 4 mm or less in width.

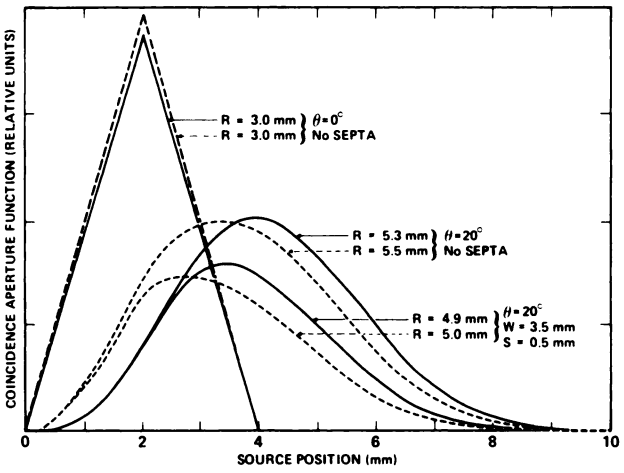

FIGURE 4
Calculated geometric coincidence aperture functions for 20-mm-deep BGO detectors with inter-crystal distance L = 4 mm. (—) Flat face; (- - -) 30° wedge

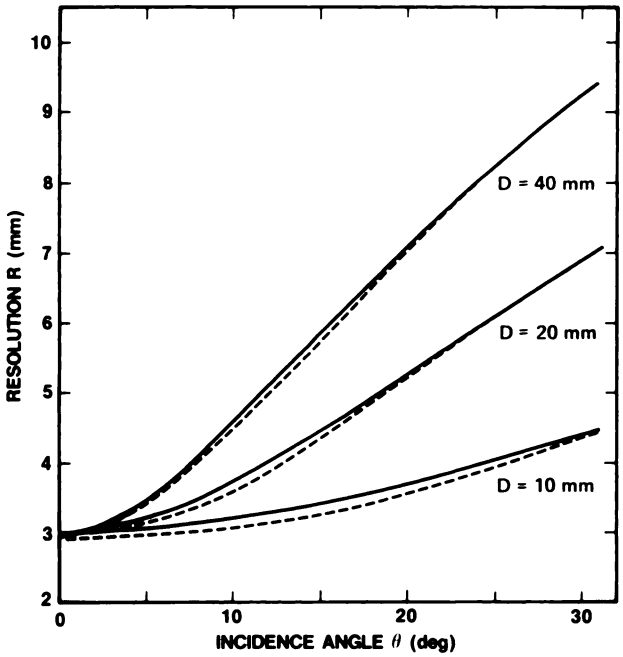

FIGURE 5
Spectral resolution vs angle of incidence on array for 4-mm-wide closely packed BGO detectors. Results are given for flat-face and wedge-shaped geometries of similar detection efficiencies. (—) Flat face; (- - -) 30° wedge; L = 4 mm without septa

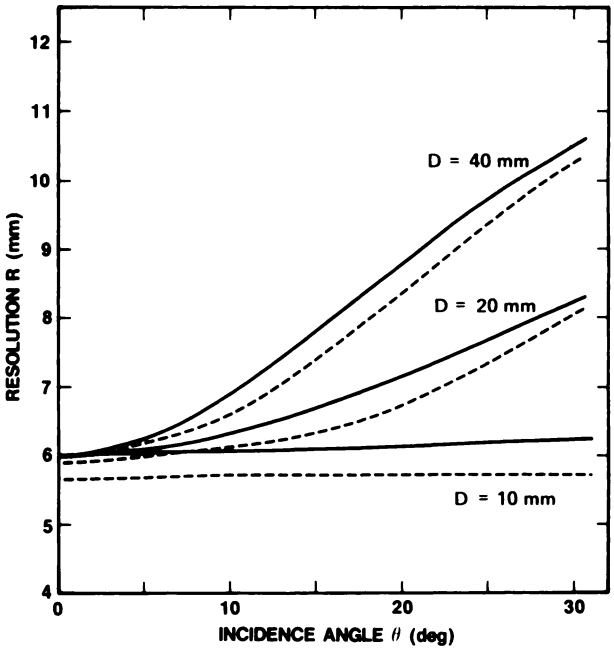

FIGURE 6
Same as Fig. 5f or 8-mm-wide detectors. (—) Flat face; (- - -) 30° wedge; L = 8 mm without septa

With Septa

To a first approximation, the effect of adding wedges to crystals is equivalent to slightly withdrawing the septa from the faces of flat crystals. It has been shown that for each angle of incidence on the array, there exists an optimum septum gap for which the best resolution and a higher detection efficiency are achieved (*8*). This remains true with tapered crystals. In Fig. 8, we compare the optimum resolution obtained with various combinations of wedge angle, septum thickness and septum gap as a function of detection efficiency for 4-mm and 8-mm interdetector distances. Wedges were assumed to be added on top of the flat crystals in these calculations. An incidence angle of $\theta = 20°$ was chosen as a compromise between the maximum angle determined by the periphery of an object in the field-of-view of a circular ring camera and the median incidence angle defined by a uniform activity distribution filling the object. There is a slight advantage in using wedge faces for an interdetector distance of L = 8 mm: improvements in resolution of ~0.4 mm are seen for constant detection efficiency, and up to 10% in detection efficiency can be gained without degrading the resolution by adding a 20° wedge. Conversely, for L = 4 mm, it is always disadvantageous to use wedge-shaped crystals since this always results in resolution loss. This is true provided that, for flat crystals, the septum is slightly receded from the face of the detector to optimize the performance. Thus, for narrow crystals, our results partly refute the analysis of Holmes and Ficke (*6*) who concluded that pointed crystals should be used in conjunction with septa.

Implicit in Fig. 8 is the existence of an interdetector distance for which the optimum resolution curves obtained with wedges and flat faces will roughly coincide. For a given angle of incidence, this point is dependent

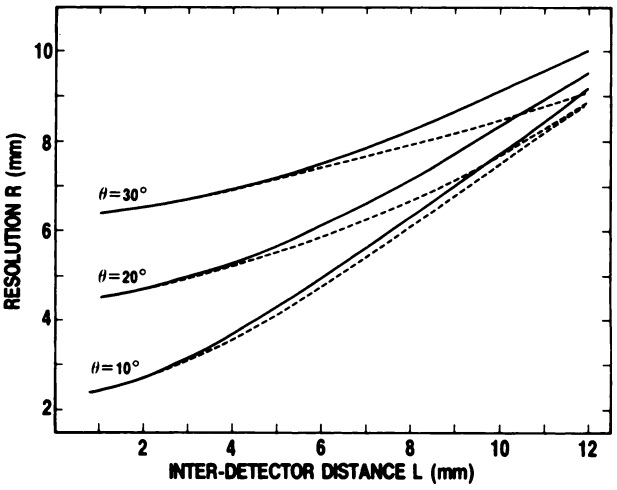

FIGURE 7
Spectral resolution vs. inter-detector distance for 10°, 20° and 30° incidence angles (BGO). Results are given for flat-face and wedge-shaped geometries of similar detection efficiencies. (—) Flat face; (- - -) 30° wedge; D = 20 mm without septa

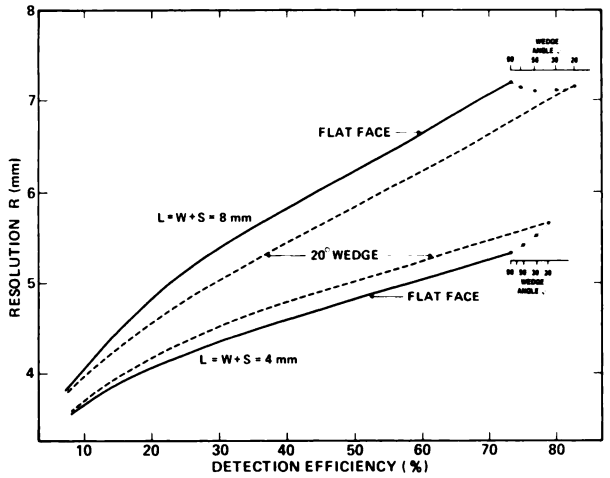

FIGURE 8
Optimum spectral resolution as function of detection efficiency for flat-face and pointed BGO crystals. Geometrical parameters that are allowed to vary in calculation of curves are septum thickness (S), septum gap (G) and wedge angle (ϕ). Tungsten septa were assumed throughout. Dotted curves at right hand side of the plot were obtained for wedges added on top of flat crystals. D = 20 mm; θ = 20°

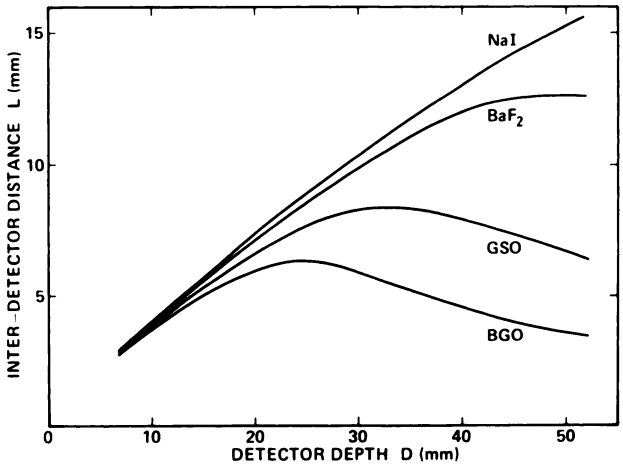

FIGURE 9
Interdetector distances for which both flat-face and pointed crystals yield to similar performance. Use of wedges must be avoided for interdetector distances smaller than those indicated by curves but should be considered for larger ones. θ = 20°

only on the crystal depth and the detector and septum materials. Therefore, the range of usefulness of wedges can be inferred from this simple argument. Figure 9 summarizes our analysis for NaI, BaF_2, GSO and BGO scintillators and tungsten septa. The curves represent the interdetector distance for which flat face and wedge-shaped crystals yield to similar performance. For larger interdetector distances, wedges become more advantageous; for smaller interdetector distances the use of pointed crystals is detrimental.

The maximum value in the curves of Fig. 9 arises from the relative importance of the crystal front end geometry with respect to the bulk of the detector volume. For shallow detectors, the wedge is a large fraction of the crystal; thus, its effect is important in that it has extra crystal depth even for rather narrow detectors. For deeper crystals (up to about twice the mean free path of 511 keV gamma rays in the detector material) wedges become useful for interdetector distances that increase steadily with respect to the crystal depth; this is in direct relation with the drop in wedge to bulk crystal ratio. As the crystal depth is further increased, the effect of the front end geometry eventually takes over again: indeed, for large crystal depths the crosstalk at angle produces a long tail on one side of the aperture function. Adding a wedge to the crystal does not significantly modify this long tail but concentrates more events in the peak of the distribution, resulting in slightly improved resolution. The gain in resolution is not worthwhile unless the interdetector distance is much larger than the boundary value given by the curves. Therefore, our conclusions for a 35-mm deep BGO detector array do not differ substantially from those of Lupton et al. (7) who recommended the use of shaped detectors only for intercrystal distances larger than ~8 mm.

CONCLUSION

Tapered crystals have been demonstrated to be inappropriate for high spatial resolution detection in PET whether or not intercrystal septa are used. It is the bulk of the detector array that is responsible for the performance of a high resolution design and the front end geometry is not significant. However, for wider detectors, wedge-shaped front faces produce higher detection efficiency and slightly improved resolution. Ironically, none of the present day medium resolution tomographs which would have gained advantages from shaped crystals incorporate this refinement. It would be advisable for the designers of such new scanners to consider the implementation of pointed crystals since this can be achieved without increasing the complexity or the cost of the system.

ACKNOWLEDGMENTS

This work was supported by the Medical Research Council of Canada and by Le Fonds de la Recherche en Santé du Québec.

REFERENCES

1. Hoffman EJ, Barton JB, Phelps ME, et al: New design concepts for quantitative positron emission tomography

of the brain. In *Positron Emission Tomography of the Brain*, Berlin, Springer-Verlag, 1983, pp 30–39
2. Burnham CA, Bradshaw J, Kaufman D, et al: A stationary positron emission ring tomograph using BGO detector and analog readout. *IEEE Trans Nucl Sci* NS-31: 632–636, 1984
3. Derenzo SE, Huesman RH, Budinger TF, et al: High resolution positron emission tomography using 3-mm wide bismuth germanate crystals. *J Nucl Med* 25: P46, 1984
4. Cho ZH, Lee HS, Hong KS: Wedge-shaped BGO scintillation crystal for positron emission tomography: concise communication. *J Nucl Med* 25: 901–904, 1984
5. Roney JM, Thompson CJ: Detector identification with four BGO crystals on a dual PMT. *IEEE Trans Nucl Sci* NS-31: 1022–1027, 1984
6. Holmes TJ, Ficke DC: Analysis of positron-emission tomography scintillation-detectors with wedge faces and inter-crystal septa. *IEEE Trans Nucl Sci* NS-32: 826–830, 1985
7. Lupton LR, Keller NA, Thompson CJ, et al: On the use of tapered bismuth germanate crystals in positron emission tomography. *Nucl Instrum Meth Phys Res* 227: 361–368, 1984
8. Lecomte R, Schmitt D, Lamoureux G: Geometry study of a high resolution PET detection system using small detectors. *IEEE Trans Nucl Sci* NS-31: 556–561, 1984
9. Nahmias C, Kenyon DB, Garnett ES: Experience with a high efficiency positron emission tomograph. *IEEE Trans Nucl Sci* NS-29: 548–550, 1982
10. Lupton LR, Keller NA: Performance study of single-slice positron emission tomography scanners by Monte Carlo techniques. *IEEE Trans Med Imaging* MI-2: 154–168, 1983.
11. Schade OH: *Image Quality: A Comparison of Photographic and Television Systems*, Princeton, RCA Laboratories, 1975
12. Wagner RF, Weaver KE, Denny EW, et al: Toward a unified view of radiological imaging systems. Part I: noiseless images. *Med Phys* 1: 11–24, 1974